Journal of Water Process Engineering 75 (2025) 107959

Contents lists available at ScienceDirect

Journal of Water Process Engineering

journal homepage: www.elsevier.com/locate/jwpe

Removal of antracene and benzo[*a*]pyrene from soil-washing synthetic emulsions by Fenton and solar photo-Fenton oxidation

Karima Ayedi [b], Yaiza Moreno-De La Fuente [a], Miguel Herraiz-Carboné [c], Salvador Cotillas [a], Marina Prisciandaro [b], Aurora Santos [a], Carmen M. Domínguez [a,*]

[a] Department of Chemical Engineering and Materials, Faculty of Chemical Sciences, Complutense University of Madrid, Avenida Complutense s/n, 28040 Madrid, Spain
[b] Department of Industrial and Information Engineering and Economics, University of L'Aquila, Piazzale Ernesto Pontieri, Monteluco di Roio, 67100 L'Aquila, Italy
[c] Department of Chemical, Energy and Mechanical Technology, ESCET, Rey Juan Carlos University, C/ Tulipan s/n, 28933 Móstoles, Madrid, Spain

ARTICLE INFO

Editor: Ludovic F. Dumée

Keywords:
AOPs
Emulsions treatment
Fenton process
PAHs
Soil washing
Solar photo-Fenton
Surfactant recovery

ABSTRACT

This study examines the treatment of polycyclic aromatic hydrocarbons (PAHs) aqueous emulsions, equivalent to those obtained from soil-washing, using Fenton and solar photo-Fenton oxidation for pollutant removal and surfactant recovery in water treatment applications. PAHs, persistent contaminants in industrial wastewater, require sustainable treatment approaches. Soil was contaminated with anthracene (ANT) and benzo[*a*]pyrene (BaP) and washed with sodium dodecyl sulfate (SDS) at a mass liquid-to-soil ratio of 2:1, with SDS concentrations ranging from 2500 to 10,000 mg L^{-1}. A synthetic emulsion (SDS: 4500 mg L^{-1}, ANT: 5 mg L^{-1}, BaP: 5 mg L^{-1}) was prepared and treated using low oxidant (H_2O_2: 60–240 mg L^{-1}) and catalyst (Fe: 2.5–10 mg L^{-1}) dosages to optimize reagent consumption. The Fenton process (pH = 3) achieved complete PAHs removal, with BaP fully degraded under all conditions and ANT requiring higher oxidant (H_2O_2, 240 mg L^{-1}) and catalyst (Fe, 10 mg L^{-1}) concentrations. The solar photo-Fenton process achieved up to 70 % ANT and 85 % BaP removal at near-neutral pH using ferrioxalate complexes (120 mg L^{-1} H_2O_2, 10 mg L^{-1} Fe). Minimal SDS degradation and negligible mineralization support surfactant recovery and reuse, enhancing process sustainability. These findings highlight the viability of light-assisted advanced oxidation processes for selective pollutant degradation in engineered water systems, supporting the development of cost-effective and environmentally friendly remediation technologies.

1. Introduction

The scientific community interest in the presence of polycyclic aromatic hydrocarbons (PAHs) in water, soil and air, has significantly increased in recent years [1]. PAHs are primarily produced by anthropogenic activities, particularly the incomplete combustion of organic materials. These persistent organic pollutants consist of two or more fused benzene rings or pentacyclic molecules and are well known for their carcinogenic, mutagenic and teratogenic properties [2]. PAHs are predominantly found in the surface layers of soil, adsorbed onto sediments or microorganisms [3–5]. Their presence has been detected in over 200,000 sites in Europe, as reported by the European Environment Agency [6]. Due to their potential risk, up to 16 PAHs have been included on the priority list issued by the United States Environmental Protection Agency (USEPA) [7]. PAHs are increasingly detected in water resources due to industrial discharge and runoff, often coexisting with other contaminants of emerging concern, such as endocrine-disrupting compounds and pharmaceuticals. This highlights the need for advanced treatment technologies capable of addressing a broad spectrum of organic pollutants. Consequently, the remediation of PAHs-contaminated sites has become a critical environmental and public health priority [8,9].

The pressing need to control PAHs has led to increased research on soil remediation technologies such as advanced oxidation processes (AOPs) [10,11]. Among these, the well-known Fenton process, which is based on the activation of H_2O_2 by ferrous iron (Fe^{2+}) to generate hydroxyl radicals (•OH) has been widely studied due to the high oxidation potential of •OH ($E^0 = 2.87$ V) [12]. The generation of •OH involves the oxidation of Fe^{2+} to Fe^{3+}, which is subsequently regenerated by its reaction with H_2O_2, thereby sustaining the catalytic cycle of H_2O_2 activation (Eqs. (1)–(2)) [13,14].

* Corresponding author.
E-mail address: carmdomi@ucm.es (C.M. Domínguez).

https://doi.org/10.1016/j.jwpe.2025.107959
Received 6 March 2025; Received in revised form 5 May 2025; Accepted 16 May 2025
Available online 20 May 2025

$$H_2O_2 + Fe^{2+} \rightarrow Fe^{3+} + HO^- + \dot{O}H \quad (1)$$

$$H_2O_2 + Fe^{3+} \rightarrow Fe^{2+} + \dot{O}OH + H^+ \quad (2)$$

This process has been successfully applied to remediate a wide range of organic contaminants in soils, including PAHs [15–18]. Smara et al. [15] treated a real soil contaminated with 16 PAHs (1200 mg kg^{-1}), including phenanthrene, fluoranthene and pyrene, among others (mass liquid-to-soil ratio $V_L/W = 3$) using a high concentration of H_2O_2 (5 M) and Fe(II) (0.5 M). A PAHs degradation ranged from 84.7 % to 99.9 % was obtained after 60 min. Gao et al. [16] applied this process to an industrial field soil contaminated with 12 PAHs (44.3 mg kg^{-1}) and lindane (γ-HCH, 19.9 mg kg^{-1}), using iron oxide particles modified by carboxymethyl cellulose supported on biochar (CMC-Fe_3O_4/BC) as catalyst (1.5 % (w/w)) and H_2O_2 as the oxidant (1 M). Around 60 % degradation of pollutants after a 10-day reaction (V_L/W mass ratio = 3) was achieved. Although promising results have been reported, it is important to emphasize that direct contact between the aqueous hydrogen peroxide solution and the contaminated soil requires excessively high concentrations of oxidant in the Fenton process—between 22 and 113 times the stoichiometric amount of H_2O_2 needed for contaminant mineralization [15,16]. This is largely due to the unproductive consumption of the oxidant by the soil, an issue that warrants improvements [19]. On the other side, the efficiency of the Fenton process is often limited by the hydrophobic nature of PAHs, which hinders their transfer from the soil to the liquid phase, reducing their interaction with the oxidizing species [20]. The use of surfactants increases the solubility of target contaminants in the aqueous phase, facilitating the mobilization of soil-adsorbed particles [21]. Surfactants can be used in washing processes for the remediation of excavated contaminated surface soils, as is usually the case of PAHs, or injected (and further extracted) into the subsurface for subsoil pollution, a process known as surfactant enhanced aquifer remediation (SEAR) [22]. Thus, direct soil treatment, which leads to a high unproductive consumption of oxidants, is avoided.

In SEAR and soil washing, the resulting emulsions, containing the pollutants, must be adequately managed [23,24]. Thus, developing oxidation treatments that enable the selective removal of PAHs from these emulsions is critical. In this regard, the Fenton process has been successfully applied to treat emulsions polluted from soil washing processes (p-cresol [25] and PAHs [26]) and SEAR (organochlorine compounds [23]) using non-ionic surfactants. One of the main drawbacks is that acidic pH is required to keep iron in solution. Unproductive oxidant consumption due to the unselective surfactant oxidation and consequently, the loss of surfactant should be also considered.

Photo-Fenton treatments have also been proposed for the removal of organic pollutants from emulsions, although only a few studies have addressed this topic. Photo-Fenton using UV lamps [27] have been applied to eliminate total petroleum hydrocarbons, and solar light has been used to remove dichlorodiphenyltrichloroethane [28]. Both studies employed non-ionic surfactants and operated under acidic pH conditions. To avoid the acid pH, solar-driven photo-Fenton, employing chelating agents like oxalate to keep iron in solution at neutral pH, has been used in aqueous phase [29–35], but there are no studies for contaminated emulsions.

The anionic surfactant sodium dodecyl sulfate (SDS) is one of the most used in soil remediation processes [36–38]. SDS is more efficient in lowering surface tension due to its strong ionic nature and presents lower adsorption onto soil particles compared to non-ionic surfactants or biosurfactants [39,40]. These benefits, alongside its wide availability and lower production costs, make SDS an attractive option for environmental applications despite some drawbacks. Additionally, due to its anionic nature, SDS presents higher stability (than non-ionic and biosurfactants) in the presence of oxidants [36,37]. Therefore, treating polluted emulsions containing SDS as surfactant with Fenton's reagent is expected to result in lower unproductive H_2O_2 consumption and higher surfactant recovery. Recycling SDS would enhance the sustainability of this anionic surfactant in the process.

To the best of the authors' knowledge, there is a notable gap in studies applying Fenton and photo-Fenton processes for degrading SDS emulsions contaminated with PAHs resulting from soil washing. Thus, this work aims to investigate the treatment of synthetic PAH-contaminated emulsions using Fenton and photo-Fenton processes, focusing on minimizing the doses of reagents (oxidant and catalyst) and maximizing the surfactant recovery. Anthracene (ANT), a 3-ring PAH, and benzo[*a*]pyrene (BaP), a 5-ring PAH, were selected as representative models of low and high-molecular-weight PAHs, respectively. The critical process variables studied include H_2O_2 and catalyst (Fe^{2+} or Fe-oxalate) concentrations, which were evaluated regarding PAH degradation, oxidant consumption, and SDS stability (a key aspect for the sustainability of the process).

2. Material and methods

2.1. Chemicals

The pollutants, anthracene (ANT, $C_{14}H_{10}$; 178.23 g mol^{-1}) and benzo[*a*]pyrene (BaP, $C_{20}H_{12}$; 252.31 g mol^{-1}), were sourced from Sigma-Aldrich. Sodium dodecyl sulfate (SDS, 90 %), also provided by Sigma Aldrich, was used as a surfactant. Hydrogen peroxide (H_2O_2, 35 %) from Thermo Scientific served as the oxidant. Iron (II) sulfate heptahydrate, from Thermo Scientific, and sulfuric acid (H_2SO_4, 98 %), from Sigma Aldrich, were employed in the Fenton tests. Sodium oxalate monohydrate (99.5 %) and iron (III) sulfate hydrate (97 %), both from Sigma Aldrich, were used to formulate the ferrioxalate complex, used as catalyst in the photo-Fenton experiments. Titanium (IV) oxysulfate solution, obtained from Sigma Aldrich, was used to quantify H_2O_2. Phenanthroline, acetic acid, ammonium acetate, and L-ascorbic acid, all from Sigma Aldrich, were used for total iron determination. Sodium tetraborate, methylene blue solution, phenolphthalein (Sigma Aldrich), and chloroform (VWR) were used for SDS quantification. HPLC-grade acetonitrile (Fisher) and phosphoric acid (Sigma-Aldrich) were used as mobile phase in HPLC determinations. All stock solutions were prepared using high-purity water from a Millipore Direct-Q system (resistivity>18 MΩ cm at 25 °C).

2.2. Soil characterization

The uncontaminated soil, taken from an industrial zone, consisted of clean industrial aggregates easily disaggregated into smaller particles (< 2 mm). The soil received was dry, so the units referring to the mass of soil expressed on an air-dry basis. The total organic carbon (TOC) of the soil was determined using a Shimadzu TOC-V analyzer. The concentration of metals was quantified using a microwave plasma atomic emission spectrometer (4100 MP-AES, Agilent). Following the EPA 3051A guidelines, soil samples were predigested in a microwave extraction system (Milestone Ethos One) using nitric (70 %) and hydrochloric (37 %) acids. The oven conditions were set to increase the temperature at 32 °C min^{-1} until reaching 175 °C, which was then maintained for 4.5 min [41]. Soil pH was determined using a Basic 20-CRISON pH electrode in a soil/water suspension (1:2, mass ratio).

To determine the concentration of PAHs in the soil, the sample was extracted with methanol (V_L/W mass ratio = 2, 180 min US, 40 °C [39]) and analyzed by HPLC.

Finally, the Natural Oxidant Demand (NOD) of the soil for H_2O_2 was assessed through a 48-h experiment in which the reference soil was mixed with 40 g L^{-1} of the oxidant (V_L/W mass ratio = 2). The concentration of H_2O_2 after this time was determined.

2.3. Soil spiking

The uncontaminated control soil (1000 g) was spiked with a concentrated solution of ANT and BaP (25 mg L^{-1} of each one) in

acetone (2000 mL, 1568 g). The mixture was then gently stirred and blended to ensure homogeneity at room temperature. After 48 h, the acetone had fully evaporated, and the soil was rinsed with Milli-Q water to remove any residual solvent. The contaminated soil was then aged for 45 days at room temperature without light. After this period, the concentration of PAHs in the soil was quantified as previously described.

2.4. Surfactant soil washing

The spiked soil was washed using different concentrations of SDS: 2500, 3500, 5000, 6500, 7500, 8500, and 10,000 mg L^{-1}, all of them above the critical micelle concentration (CMC) of the anionic surfactant (established at approximately 1800 mg L^{-1} [42]). The surfactant solution was added to the polluted soil at a V_L/W mass ratio of 2:1 in PTFE vials and stirred for 24 h, sufficient time to reach equilibrium conditions [36]. The PTFE vials were then centrifuged at 9000 rpm to separate the two phases: soil and polluted emulsion. Subsequently, the concentration of SDS and the solubilized PAHs were measured in the aqueous phase, and the remaining concentration of pollutants was measured in the soil phase. The experiments were performed by triplicate.

2.5. Treatment of synthetic polluted emulsions

Once the initial concentration of SDS was selected to wash the soil (10,000 mg L^{-1}, which resulted in an emulsion with a surfactant concentration of around 4500 mg L^{-1} and contaminants of around 5 mg L^{-1} of each), a synthetic emulsion reproducing these conditions was prepared.

It is important to note that, for practical reasons, synthetic emulsions were used for oxidation experiments instead of real emulsions obtained from the soil washing process. The experimental setup required large volumes of emulsion (up to 2 L per test), which, including replicates and variable optimization, would demand over 70 L of emulsion and >35 kg of contaminated soil. Generating this amount of real emulsion under consistent conditions in a single batch was not feasible. Therefore, a synthetic emulsion was prepared to closely replicate the composition obtained from the washing process, ensuring experimental consistency across all tests.

For that purpose, a surfactant solution with the required SDS concentration (4500 mg L^{-1}) and pollutants (5 mg L^{-1} ANT, and 5 mg L^{-1} BaP) was prepared. The mixture was vigorously agitated for 72 h to ensure complete pollutant dissolution.

The synthetic emulsion was treated using Fenton and photo-Fenton processes. Fenton experiments were conducted in batch mode using a 500 mL amber reagent glass bottle to minimize the influence of light exposure and immersed in a bath for temperature control placed on a stirrer plate. A solar light simulator with a cylindrical borosilicate glass flat-plate reactor with external recycling (380 mL, 10 cm length) was used for solar photo-Fenton experiments. The reactor featured a quartz window to ensure effective UV–Vis radiation transmission. The light source was an Oriel 67,005 solar simulator, equipped with an air mass filter (AM 1.5 G, ASTM E 892 standard) and a liquid attenuation filter (Water Optical Filter, 1.5 Inch Series) provided by Newport Corp. The working power was fixed at 240 W and the distance between the light source and the reactor window (diameter = 7 cm) was 10 cm, giving an irradiance value of 6.2 W cm^{-2}. This configuration simulates the average solar radiation in Madrid (40°30′ N, 3°40′ E, Spain) on a clear September day, with standard relative humidity conditions (40–60 %). The spectrum of the simulated solar light irradiated through the reactor quartz window is shown in the Supplementary material, Fig. SM1. The synthetic emulsion (2 L), containing contaminants, catalyst and oxidant, was recirculated (3 L min^{-1}) using a liquid pump (NF 300 KT, Liquiport) ensuring good mixing conditions. A circulating-thermostatic system (Temperature controller, PolyScience) maintained a consistent temperature throughout the reaction. More details about the experimental setup can be found elsewhere [43].

The oxidation experiments (both in Fenton and photo-Fenton tests) were conducted by first adding the synthetic emulsion to the reactor, secondly, the catalyst, and finally, the oxidant. The effect of oxidant (H_2O_2: 60–240 mg L^{-1}) and catalyst (Fe: 2.5–10 mg L^{-1}) concentration was studied in both systems. Control experiments were also performed.

The required concentration of H_2O_2 for the mineralization (conversion to carbon dioxide and water) of ANT and BaP was calculated based on their respective stoichiometric reactions with hydroxyl radicals (Eqs. (3) and (4)), assuming that each mole of hydrogen peroxide yields one mole of hydroxyl radical (Eq. (1)).

$$C_{14}H_{10} + 66\dot{O}H \rightarrow 14\ CO_2 + 38\ H_2O \tag{3}$$

$$C_{20}H_{12} + 92\dot{O}H \rightarrow 20\ CO_2 + 52\ H_2O \tag{4}$$

The resulting hydrogen peroxide concentrations for 5 mg L^{-1} of ANT and BaP were 63 and 62 mg L^{-1}, respectively, leading to a combined value of approximately 120 mg L^{-1}. To evaluate the effect of oxidant dosage, lower (60 mg L^{-1}) and higher (240 mg L^{-1}) concentrations were also tested. These concentrations are significantly lower than those used when the Fenton process was directly applied to directly treat PAHs-contaminated soils (between 22 and 113 times the stoichiometric amount of H_2O_2 [15,16]), significantly softening the reaction conditions and lowering the costs.

The iron concentrations were chosen based on the maximum limit permitted by the Spanish government for environmental discharge (10 mg L^{-1}) [44]. Thus, iron concentrations of 10, 5, and 2.5 mg L^{-1} were used within the regulatory limits. In the Fenton tests ($pH_0 = 3$), ferrous iron (Fe^{2+}, previously dissolved in acidified water, H_2SO_4) was used as a catalyst, while in the photo-Fenton experiments (pH = 6.5–7), ferric iron (Fe^{3+}), in the form of a ferrioxalate complex, was employed [45]. This compound prevents iron precipitation when operating under circumneutral pH conditions [29,30]. The ferrioxalate complex is formed from iron (Fe^{3+}) and oxalate (Eq. (5)). An oxalate/iron molar ratio of 10:1 was selected to ensure complete iron solubilization.

$$Fe^{3+} + 3C_2O_4^{2-} \rightleftarrows \left[Fe(C_2O_4)_3\right]^{3-} \tag{5}$$

Under solar light irradiation, Fe^{3+} (from the ferrioxalate complex) is reduced to Fe^{2+} (Eq. (6)), facilitating the catalytic decomposition of hydrogen peroxide to generate hydroxyl radicals (Eqs. (1)–(2)).

$$\left[Fe(C_2O_4)_3\right]^{3-} \xrightarrow{h\nu} Fe^{2+} + 2C_2O_4^{2-} + C_2O_4^{-} \tag{6}$$

The operation conditions for these experiments are summarized in Table 1. To study the effect of hydrogen peroxide concentration in both Fenton and solar photo-Fenton processes, maintaining the other variables constant, the intermediate Fe concentration (5 mg L^{-1}) was used as a constant. On its side, when assessing the effect of iron concentration, 120 mg L^{-1} of H_2O_2 was used. Based on previous works, the experimental time was set to 360 min. The pH was continuously monitored throughout the experiment. To track the progress of the reaction, 5 mL aliquots were collected at various reaction times (0, 30, 60, 120, 180, 240, 300, and 360 min) using a syringe. After performing the necessary dilutions, the samples were analyzed using different instruments to monitor the temporal evolution of the contaminants, hydrogen peroxide and Fe concentration. Moreover, the stability of the surfactant (and its possible reuse) was evaluated at the end of the reaction time through SDS and TOC concentration measurements.

The surfactant activity of SDS depends on both the sulfonate groups and the alkyl chain, making the integrity of both critical to maintaining its functionality. Thus, the surfactant capacity was indirectly measured by quantifying sulfate and sulfonate groups (SDS concentration) and the integrity of the alkyl chain (the hydrophobic portion of the surfactant, through total organic carbon (TOC) analysis). Moreover, the surfactant capacity of selected treated emulsions (120 mg L^{-1} of H_2O_2 and 5 mg L^{-1} of Fe) was assessed by measuring the superficial tension and the critical micelle concentration (CMC) and compared to the initial emulsion.

Table 1
Experimental conditions for treating synthetic emulsions (4500 mg L^{-1} of SDS and 5 mg L^{-1} of BaP and ANT).

Exp. (E)	Test	Light source	pH_0	Iron source	$[Fe]_0$ (mg L^{-1})	$[H_2O_2]_0$ (mg L^{-1})
1	Control	–	6.5–7	–	0	0
2	Control	–	6.5–7	–	0	120
3	Control	–	3	$FeSO_4$	5	0
4	Fenton	–	3	$FeSO_4$	5	60
5					5	120
6					5	240
7	Fenton	–	3	$FeSO_4$	2.5	120
5					5	120
8					10	120
9	Control	–	6.5–7	$[Fe(C_2O_4)_3]^{3-}$	5	0
10	Control	–		$[Fe(C_2O_4)_3]^{3-}$	5	120
11	Control	Solar lamp		–	0	0
12	Control	Solar lamp		–	0	120
13	Photo-	Solar	6.5–7	$[Fe(C_2O_4)_3]^{3-}$	5	60
14	Fenton	lamp			5	120
15					5	240
16	Photo-	Solar	6.5–7	$[Fe(C_2O_4)_3]^{3-}$	2.5	120
14	Fenton	lamp			5	120
17					10	120

All experiments were carried out at room temperature in triplicate.

2.6. Analytical methods

The concentration of PAHs (in the organic phase obtained from soil extraction and in the emulsions, both real and synthetic) was determined by HPLC equipped with an Agilent 1100 series-coupled DAD detector and a Poroshell 120 EC-C18 2.7 μm (3.0 × 150 mm) column, at 40 °C. The mobile phase (0.5 mL min^{-1}) consisted of acetonitrile (HPLC-grade) and 0.1 % phosphoric acid (60:40 %, v:v). An injection volume of 20 μL was employed. A 250 nm and 300 nm wavelength were used for ANT and BaP determination, respectively.

The total organic carbon (of soil and real and synthetic emulsions) was determined using a Shimadzu TOC-V analyzer with an infrared detector. Total carbon (TC) was measured through oxidative combustion at 714 °C. Inorganic carbon (IC) was determined at 200 °C after adding phosphoric acid (35 %) to the soil sample.

The concentration of H_2O_2 (in the synthetic emulsions and in the NOD determination) was quantified by measuring the concentration of the complex formed between H_2O_2 and Ti^{4+}, using titanium (IV) oxysulfate solution. The concentration of this complex was then analyzed spectrophotometrically at 410 nm [46]. Total iron concentration in the synthetic emulsions was measured following ISO 6332 guidelines. This colorimetric method involves adding 1 mL of 1,10-phenanthroline, 1 mL of acetic acid (7.32 g L^{-1}), and ammonium acetate (250 g L^{-1}) to 4 mL of the sample. The resulting solution was analyzed spectrophotometrically at 510 nm to quantify ferrous iron (Fe^{2+}). Ferric iron (Fe^{3+}) was subsequently determined at 510 nm by adding L-ascorbic acid [47]. Total iron is the sum of ferrous and ferric iron concentration.

The concentration of oxalate (from ferrioxalate complex) in the emulsions corresponding to photo-Fenton experiments was determined by ion chromatography (IC). Ions were measured using a Metrohm 930 Compact IC Flex connected to a conductivity detector and a Metrosep A Supp 5250/4.0 column. The mobile phase (0.7 mL min^{-1}) consisted of Na_2CO_3 (3.2 mM) and $NaHCO_3$ (1 mM). The injection volume was 20 μL. Conductivity and pH were measured using a HI991301 pH/EC/TDS Meter supplied by Hanna.

SDS concentration was determined by a spectrophotometric method based on forming an ionic pair between the anionic surfactant and methylene blue [48]. A buffer was prepared with 10 mM sodium tetraborate ($Na_2B_4O_7 \cdot 10H_2O_2$). First, 200 μL of the buffer was added to 5 mL of the SDS-containing sample. Then, 30 μL of methylene blue solution (0–2.5 mg L^{-1}) and 50 μL of phenolphthalein were added to the buffer-SDS complex. After mixing for 5 min, the anionic surfactant–cationic dye complex was extracted with chloroform (4 mL), and the extract was measured at 650 nm (Spectroquant® Prove 300 UV/VIS Spectrophotometer, Merck Millipore). The surface tension and the critical micelle concentration (CMC) of the synthetic emulsions (before and after oxidation treatments) was determined using a Force Tensiometer (Tensíío KRÜSS WO04779). The CMC is automatically determined through a series of surface tension measurements at varying surfactant concentrations. The equipment performs successive dilutions of the sample and records the corresponding surface tension values. As the surfactant concentration increases, the surface tension decreases until it reaches a plateau (this point indicates the onset of micelle formation). The CMC is identified as the concentration at which further increases in surfactant no longer result in significant changes in surface tension. The CMC is calculated from the inflection point in the surface tension *vs.* concentration curve.

3. Results and discussion

3.1. Soil characterization

The uncontaminated soil was primarily composed of fine silts and clays. The soil exhibited a near-neutral pH, an inorganic carbon content (bicarbonate) of 189.36 ± 3.89 g $kg^{-1,}$ and an organic carbon content of 17.87 ± 1.21 g kg^{-1}, likely associated with the presence of humic acid-type compounds [41]. The concentration of metals in the soil is summarized in Table SM1, with calcium and copper being the most prevalent. Residual amounts of silicon, magnesium, and potassium were also detected.

The calculated NOD of the soil exceeded 120 g of H_2O_2 per kg of soil, primarily due to the high carbonate content of the soil [41]. This substantial unproductive consumption of H_2O_2 indicates that the direct use of this oxidant is unsuitable for remediating soils with these characteristics, underscoring the need first to wash the soil to extract pollutants and subsequently treat the soil washing solution.

After the soil spiking and ageing processes, the concentration of contaminants determined in the soil was 35.12 ± 3.15 mg kg^{-1} of ANT and 14.64 ± 1.20 mg kg^{-1} of BaP. The other soil characteristics (concentration of metals, TOC, IC, pH and NOD) remained unchanged (data here not shown).

3.2. Surfactant soil washing

As stated, soil washing processes were conducted using initial SDS concentrations of 2500, 3500, 5000, 6500, 7500, 8500, and 10,000 mg L^{-1}. The concentration of SDS in the soil washing solutions after the washing process (24 h) was determined by the spectrophotometric method. Based on the initial and final SDS concentrations and considering the mass-based aqueous phase/soil ratio used (2:1), the amount of SDS adsorbed onto the soil was determined. This value, denoted as q, expressed in grams of SDS adsorbed per kilogram of soil.

The results of q plotted against the concentration of SDS in the real emulsions ($SDS_{emulsion}$), resulting from the soil washing process, are shown in Fig. 1a (adsorption isotherm of SDS in soil). The residual concentration of PAHs in the soil and dissolved in the washing emulsions were measured with the mass balance of pollutants achieved (>90 %) for all SDS concentrations. The partition coefficients (K_d, L kg^{-1}), representing the ratio between the concentration of each PAH in the soil ($PAH_{i,soil}$, mg kg^{-1}) and the aqueous phase ($PAH_{i,aq}$, mg L^{-1}) at equilibrium conditions (24 h), were calculated using Eq. (7). The dependence of the partition coefficients for ANT and BaP on the SDS concentration is shown in Fig. 1b.

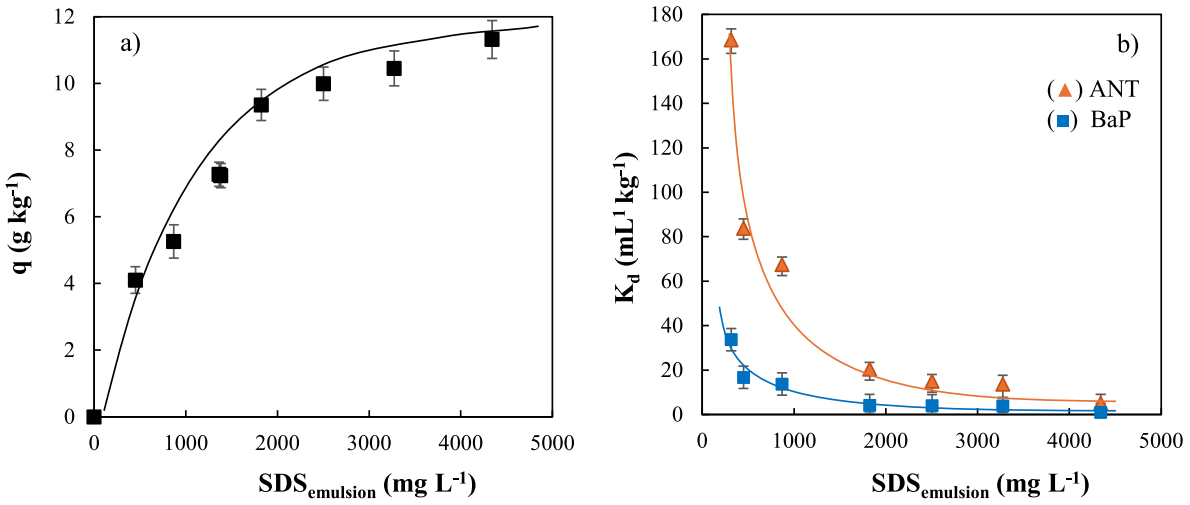

Fig. 1. a) Adsorption isotherm of SDS in the contaminated soil and, b) K_d of ANT and BaP after soil washing with SDS (V_L/W mass ratio = 2, 24 h) (mean values ± standard deviations).

$$K_d = \frac{[PAH_i]_{soil}}{[PAH_i]_{aq}} \quad (7)$$

Soil washing led to the adsorption of some surfactant [49], with a non-linear partition of SDS between soil and liquid phases (Fig. 1a), reaching asymptotic values, as usually reported in the literature for anionic surfactants [50]. SDS adsorption increased from 4.10 to 11.60 g kg^{-1} of soil as the initial SDS concentration rose from 2500 to 10,000 mg L^{-1} (final SDS in the aqueous phase from 500 to 4500 mg L^{-1}, respectively). Soil physicochemical and mineralogical properties influence surfactant adsorption [51], particularly the kaolinite content [51]. A wide range of results has been published regarding SDS adsorption on soils (1.8 g kg^{-1} when initial SDS was 5000 mg L^{-1} [36] to 11 g kg^{-1}, when initial SDS was 10,000 mg L^{-1} [50]). From these studies it can be concluded that the type and concentration of contaminants also affect the SDS adsorption [50]. Although a fraction of the SDS remains adsorbed onto the soil, this effect is considered manageable, especially in the context of industrial soil remediation, where the treated soil undergoes a clear improvement and can be rinsed prior to being returned to the site.

Despite the partial loss of surfactant due to adsorption, surfactants play a crucial role in the remediation of PAH-contaminated soils, as they significantly enhance the solubility of PAHs, which are otherwise poorly soluble in water (*e.g.*, ANT and BaP solubility = 0.044 mg L^{-1} [52] and BaP = 0.0038 mg L^{-1} [53]). Without surfactants, a partition coefficient higher than 1300 L kg^{-1} was obtained for the two pollutants (data not included in Fig. 1b), which would excessively increase the reaction volume to be treated and therefore, slow down soil remediation process.

As shown in Fig. 1b, adding SDS significantly increased PAHs solubilization, reducing the K_d of the two pollutants and enhancing contaminant removal. When the concentration of SDS in the soil washing emulsion exceeded 4000 mg L^{-1} (initial SDS concentration of 10,000 mg L^{-1}), the PAH partition coefficient remained constant, with the value for ANT (5.05 L kg^{-1}) being five times higher than that for BaP (1.03 mg L^{-1}).

The concentration of iron in the soil washing emulsion, determined by colorimetry, was negligible. This is particularly relevant since iron plays a crucial role as a catalyst in the Fenton-type processes intended for treating these emulsions.

Considering the SDS partitioning between soil and aqueous phase (Fig. 1a) and the increase in PAHs solubility with SDS concentration in the soil washing emulsion at the tested V_L/W mass ratio used (Fig. 1b), an initial concentration of SDS of 10,000 mg L^{-1} was selected.

Following this experiment, a real emulsion with a SDS concentration of 4341.72 mg L^{-1}, above the CMC of this surfactant, and 6.15 mg L^{-1} of ANT and 4.31 mg L^{-1} of BaP was obtained. At these conditions (V_L/W mass ratio = 2, 24 h), the remaining concentration of pollutants in the soil was 19.05 and 5.38 mg kg^{-1} of ANT and BaP, respectively. In the tested conditions (V_L/W = 2 mL g^{-1}, 24 h). Thus, 51 % of total PAHs were extracted in the soil washing process, suggesting that successive cycles would be needed its complete remediation [28,36]. The adsorption of SDS is expected to decrease with subsequent soil washing cycles, which would lower the amount of surfactant needed [36].

3.3. Treatment of synthetic emulsions

Based on the K_d values obtained from the soil washing experiments, a synthetic polluted emulsion containing 4500 mg L^{-1} of SDS, 5 mg L^{-1} of ANT, and 5 mg L^{-1} of BaP was prepared.

3.3.1. Fenton process: effect of oxidant and catalyst dosage

Control experiments were conducted to assess the stability of the pollutants in synthetic emulsion. Three scenarios were tested: emulsion without any reagents (E1), with the oxidant (H_2O_2, E2), and with the catalyst (Fe, E3). The reaction mixture was gently agitated, and the concentration of PAHs was monitored over 6 h. The normalized concentration of ANT and BaP at the end of the experiments are presented in Fig. 2.

The concentration of PAHs in the emulsion remained stable (E1), ruling out the possibility of PAHs volatilization at room temperature. Similarly, no significant change in the concentration of PAHs was detected when iron was added to the emulsion (E3). The addition of H_2O_2 led to a slight decrease in the concentration of ANT and BaP (<10 %), likely due to the oxidation potential of H_2O_2 (E^0 = 0.87 V) [15,54,55]. The minimal degradation of contaminants under these conditions highlights the need to activate the oxidant to generate more reactive species, such as hydroxyl radicals (E^0 = 2.87 V) [12], generated in the Fenton process. The effectiveness of this process on PAHs degradation was assessed using different doses of hydrogen peroxide (E4, E5 and E6), maintaining a constant concentration of catalyst (5 mg L^{-1} of Fe) and catalyst (E7, E5 and E8), with a constant concentration of H_2O_2 (120 mg L^{-1}). The conversion of ANT and BaP (X_{ANT} and X_{BaP}, respectively), calculated with Eq. (8), over reaction time at different concentrations of H_2O_2 are plotted in Fig. 3a and b, respectively.

$$X = \frac{C_{i,0} - C_{i,t}}{C_{i,0}} \quad (8)$$

The pollutants were progressively degraded over time using lower

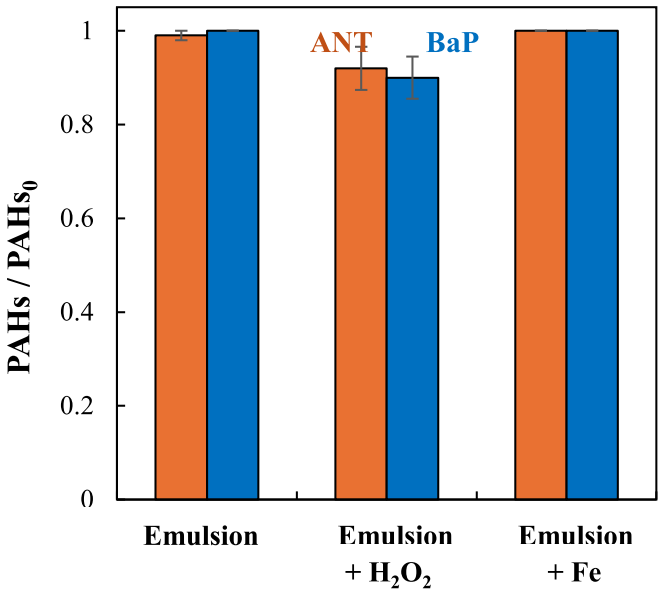

Fig. 2. Normalized concentration of PAHs in the synthetic emulsions (4500 mg L^{-1} of SDS, 5 mg L^{-1} of ANT and 5 mg L^{-1} of BaP) without reagents (E1), in the presence of H_2O_2 (120 mg L^{-1}, E2), and Fe (5 mg L^{-1}, E3) (mean values ± standard deviations).

oxidant concentrations than those reported in literature for the direct application of Fenton's reagent on soil or non-ionic surfactant [15,16,26]. Results in Fig. 3a and b show a rapid conversion of PAHs during the first 60 min, followed by a slower degradation rate. This behavior could be due to hydroxyl radicals competing to oxidize intermediate organic compounds and the parent compounds (ANT and BaP) [32] from this time. In general, increasing the oxidant dosage accelerates PAH degradation due to enhanced generation of hydroxyl radicals. However, this relationship is not linear indefinitely, as excessively high concentrations of H_2O_2 can have counterproductive effects. Specifically, with H_2O_2 concentrations of 60, 120, and 240 mg L^{-1}, complete degradation of BaP was achieved after 120, 180, and 240 min, respectively (Fig. 3b). Additionally, complete degradation of ANT was achieved in 120 min at the highest oxidant dose (Fig. 3a). The generation of hydroxyl radicals increases as the concentration of H_2O_2 (Eqs. (1)–(2)) increases, resulting in higher hydroxyl radicals production and faster pollutant degradation. Nevertheless, excess hydrogen peroxide can also act as a scavenger of hydroxyl radicals (•OH), reacting to form hydroperoxyl radicals (•OOH), with a significantly lower oxidation potential ($E^0 = 1.70$ V). This side reaction reduces the concentration of reactive radicals available for pollutant oxidation. Additionally, high concentrations of H_2O_2 can react with Fe^{2+}, producing Fe^{3+} without generating additional •OH, thereby reducing the overall catalytic efficiency of the Fenton system. These competing reactions highlight the importance of optimizing the H_2O_2 dosage to maximize degradation while minimizing scavenging effects.

The effect of catalyst concentrations on PAHs removal was evaluated using 120 mg L^{-1} of H_2O_2. The degradation of PAHs with 2.5, 5, and 10 mg L^{-1} of Fe is shown in Fig. 4. Increasing iron concentration enhanced the degradation of contaminants. BaP degradation occurred faster than ANT across all tested iron concentrations. Specifically, the complete degradation of BaP and ANT was achieved after 120 and 300 min, respectively, with 10 mg L^{-1} of Fe. Similar trends were observed for lower catalyst dosages (5 and 2.5 mg L^{-1} of Fe). Using the maximum concentration of catalyst tested (10 mg L^{-1} of Fe), complete degradation of BaP required approximately 180 min (Fig. 4a), and over 80 % of ANT was removed after 360 min (Fig. 4b). The presence of iron facilitated the catalytic cycle of H_2O_2 decomposition generating hydroxyl radicals (Eqs. (1)–(2)), which oxidize the organic contaminants during the Fenton reaction [56,57]. Therefore, higher iron concentrations may increase hydroxyl radical production and enhance the rate of PAH removal.

Regarding reagents consumption, oxidant, catalyst, and pH evolution were monitored during reactions (data not shown). Regardless the initial oxidant concentration (60, 120 and 240 mg L^{-1}), H_2O_2 consumption remained below 30 % at 6 h under all tested conditions (E4-E8). It is worth noting that this consumption is primarily attributable to the PAHs, as confirmed by an additional control experiment conducted in the absence of PAHs (4500 mg L^{-1} SDS, 120 mg $L^{-1}H_2O_2$, and 5 mg L^{-1} Fe, not included in the figures or experimental summary table). In this test, H_2O_2 consumption after 6 h of reaction was only 3.7 %, confirming that SDS contributes minimally to oxidant depletion under the conditions evaluated. The pH remained around 3 throughout the 6-h experiment, preventing iron precipitation. Thus, the dissolved iron concentration (ferric + ferrous iron) showed no significant change.

3.3.2. *Solar photo-Fenton process: effect of oxidant and catalyst dosage*

The treatment of PAHs-contaminated emulsions using the photo-Fenton process at neutral pH was evaluated to address the challenges associated with the acidic pH required in the Fenton process. As previously stated, a ferrioxalate complex was used for preventing iron

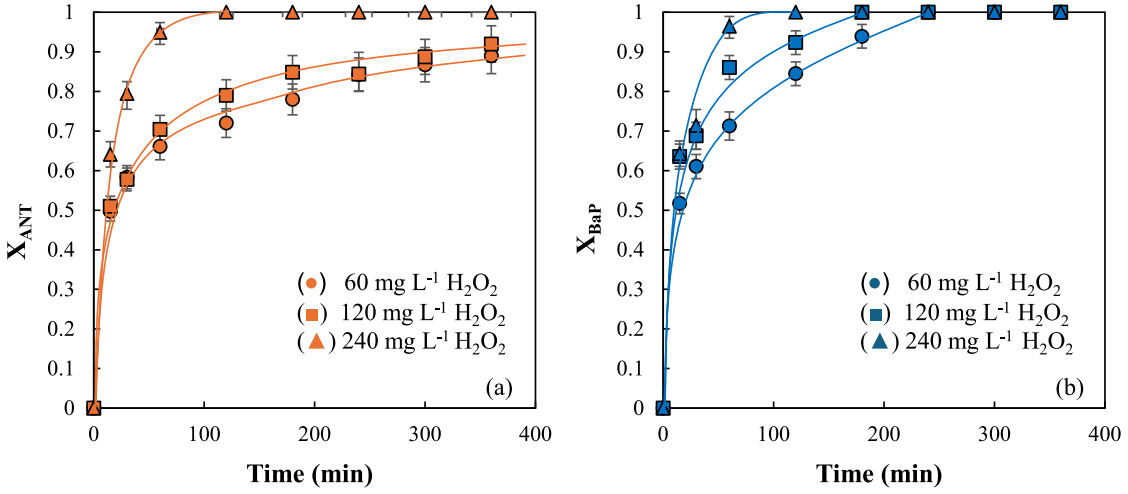

Fig. 3. Influence of H_2O_2 concentration on the degradation of PAHs in the emulsion by Fenton process (E4–E6) (4500 mg L^{-1} of SDS, 5 mg L^{-1} of ANT, 5 mg L^{-1} of BaP and 5 mg L^{-1} of Fe, pH = 3, mean values ± standard deviations).

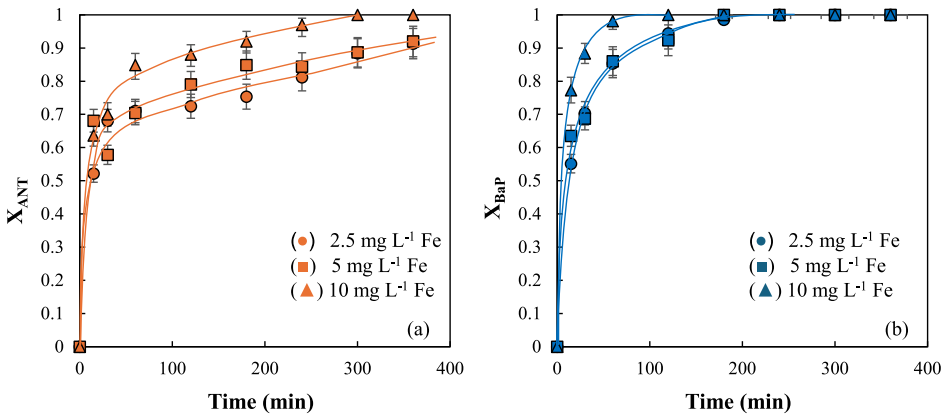

Fig. 4. Influence of iron concentration on the degradation of PAHs in the emulsion in the Fenton process (E5, E7, E8) (4500 mg L^{-1} of SDS, 5 mg L^{-1} of ANT, 5 mg L^{-1} of BaP and 120 mg L^{-1} of H_2O_2, pH = 3, mean values ± standard deviations).

precipitation at circumneutral pH [29,30]. For this reason, solar photo-Fenton experiments at acidic pH were not considered, as the main advantage of this system lies precisely in enabling photo-Fenton reactions under near-neutral conditions, thus avoiding the limitations associated with acidic operation.

First, a series of control experiments were conducted to assess the chemical stability of the PAHs under different conditions: in the presence of the ferrioxalate complex (E9), with both ferrioxalate and H_2O_2 (E10) and under solar light irradiation (E11) and in the presence of the ferrioxalate complex and solar light irradiation (E12). The remaining concentrations of PAHs after the 6 h of treatment are shown in Fig. SM2. In the absence of light, the ferrioxalate complex had a negligible effect on PAHs degradation (E9). Similarly, when H_2O_2 and the ferrioxalate complex were present (E10), minimal degradation of ANT and BaP (<10 %) was achieved at neutral pH (Fig. SM2). Under these conditions, the ferrioxalate complex does not generate Fe^{2+}, thereby minimizing the catalytic decomposition of H_2O_2 to hydroxyl radicals at circumneutral pH. The slight PAHs degradation observed may be attributed to the oxidation potential of H_2O_2, which has been shown to degrade PAHs to a certain extent [15,54,55], as previously observed in control test E2.

Organic pollutants can also be degraded through direct light irradiation within a spectrum range [58,59]. The potential of simulated solar light irradiation to degrade the target PAHs was evaluated in E11. First, the absorption spectra of ANT and BAP were determined. Both compounds exhibit a broad absorption spectrum, primarily in the UV range from 190 to 450 nm (Fig. SM3). As the solar simulator reactor emits from 350 nm (Fig. SM1), these compounds could be partially degraded under solar light irradiation. Specifically, about 15 % of the total radiation from the solar simulator falls within the 350 to 450 nm range. The evolution of PAHs concentration during photolysis with simulated solar radiation (E11) revealed a slight decrease, with ANT and BaP concentrations reduced by approximately 12 and 22 % after 6 h, respectively (Fig. SM2). This modest degradation highlights the convenience of combining solar radiation with other technologies such as the Fenton process. Finally, the combination of simulated solar radiation and hydrogen peroxide did not significantly enhance the degradation of the contaminants (E12: 15 % and 23 % for ANT and BaP, respectively, after 6 h of reaction) compared to solar radiation alone (E11: 12 % and 22 %) or hydrogen peroxide alone (E2: 8 % and 10 %). These results confirm that the presence of iron is essential to activate the decomposition of hydrogen peroxide into hydroxyl radicals.

The key operating variables in the solar photo-Fenton oxidation treatment (oxidant and iron dosages) were evaluated. The conversion of ANT and BaP at initial H_2O_2 concentrations from 60 to 240 mg L^{-1} are presented in Fig. 5a and b, respectively.

A clear positive effect of the solar photo-Fenton process compared to direct photolysis (E11) was observed, with final PAHs degradations increasing by approximately 30 %. A slight increase in the degradation rate of the pollutants was noted as the oxidant concentration increased. ANT degradation ranged from 28 to 39 % (Fig. 5a) and BaP from 51 to 59 % (Fig. 5b) when using H_2O_2 concentrations from 60 to 240 mg L^{-1}. These results also confirm the preferential degradation of BaP over ANT during the simulated solar photo-Fenton process at neutral pH.

The limited improvement in PAHs degradation with increased oxidant dosage could be attributed to an unproductive reaction among oxidants and radicals when the oxidant concentration increases [30].

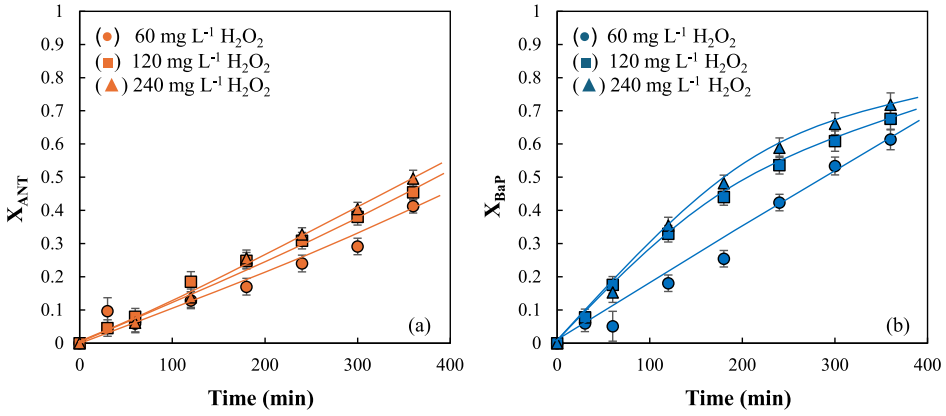

Fig. 5. Influence of H_2O_2 concentration on the degradation of PAHs in the solar photo-Fenton process (E13–E15) (4500 mg L^{-1} of SDS, 5 mg L^{-1} of ANT, 5 mg L^{-1} of BaP and 5 mg L^{-1} of Fe, pH = 7, mean values ± standard deviations).

The effect of catalyst concentration was evaluated, maintaining the concentration of the oxidant. PAHs conversions with time obtained with Fe concentrations (in the form of ferrioxalate complex) ranging from 2.5 to 10 mg L^{-1} are shown in Fig. 6.

The results demonstrated an increase in ANT degradation from 30 to 69 % over 6 h when the iron dosage was raised from 2.5 to 10 mg L^{-1} (Fig. 6a). Similarly, BaP degradation improved significantly, from 64 to 86 %, with the same increase in catalyst dosage (Fig. 6b). These findings suggest that PAHs degradation in the photo-Fenton process is more influenced by catalyst than by initial oxidant concentration [30]. This effect is likely due to the higher production of Fe^{2+} in the solution, leading to an increased generation of hydroxyl radicals. Therefore, it would be beneficial to use higher catalyst concentrations or extend the reaction time to enhance PAH degradation.

Regarding reagent consumption, the evolution of H_2O_2, Fe^{2+}, and oxalate concentration was monitored during the solar photo-Fenton tests (data not shown). The oxidant consumption (H_2O_2) was below 25 % under all tested conditions (E13-E-17), slightly lower than the corresponding Fenton tests. Consistent with the observations in the Fenton process, the low hydrogen peroxide consumption was attributed to the presence of PAHs rather than to SDS. Additionally, there was a negligible variation in total iron concentration, as the oxalate concentration at the final reaction time (above >75 % of the initial oxalate) was sufficient to sustain the formation of the ferrioxalate complex (Eq. (5)). Finally, a neutral pH between 6 and 7 was maintained through the 6-h experiments, which is a great advantage from the point of view of the application of the process.

3.3.3. Comparison of Fenton and solar photo-Fenton processes

The data obtained from the removal of PAHs during the Fenton and simulated solar photo-Fenton processes were fitted to a pseudo-first-order kinetic model (Eq. (9)), and the corresponding apparent pseudo-first-order rate constants and correlation coefficients are summarized in Table SM2. This approach is justified by the relatively small variations in the concentrations of both the oxidant and the catalyst throughout the reaction time (<30 % and 10 %, respectively), allowing their effects to be incorporated into the apparent rate constant.

$$Ln(C_0/C_t) = k_{app} \cdot t \quad (9)$$

where, C_0 represents the initial concentration of PAHs (5 mg L^{-1}), C_t is the PAHs concentration (mg L^{-1}) at a given time, k_{app} is the apparent pseudo-first-order rate constant (h^{-1}), and t is the reaction time (h).

As expected, the apparent pseudo-first-order rate constants for PAHs degradation increased with higher concentrations of both oxidant and catalyst in both technologies. The fit to a first-order reaction was less accurate when using data from Fenton's process (pH 3) than simulated solar photo-Fenton. In the last one, changes in catalyst concentration had a greater influence on the variation of the pseudo-first-order rate constants than the hydrogen peroxide dosage. BaP exhibited higher pseudo-first-order rate constants than ANT under all operating conditions, despite its more complex structure (5 rings) compared to anthracene (3 rings).

Finally, the Fenton process demonstrated approximately twice the degradation kinetics compared to the solar photo-Fenton process, confirming that the first one may offer a faster alternative for PAHs degradation but with drawback of acidic pH.

The total PAHs degradation achieved (%) by the end of the experimental time for both technologies is summarized in Fig. 7. As shown, BaP is completely degraded by the Fenton process under all conditions tested. In the case of ANT, 120 mg L^{-1} of H_2O_2 and ≥ 5 mg L^{-1} of Fe were necessary.

Under equivalent conditions, the simulated solar photo-Fenton process showed more moderate results, with ANT removal ranging from 35 to 70 % and BaP from 60 to 85 % across the different operating conditions studied.

Overall, the Fenton process consistently achieved higher final degradation rates for both ANT and BaP compared to the simulated solar photo-Fenton process under all tested conditions.

Notably, in both technologies, the degradation of BaP is faster than ANT at the different oxidant and catalyst dosages. Previous studies have suggested that the characteristics of PAHs influence degradation efficiencies in Fenton oxidation. Generally, low molecular weight PAHs (2–3 rings) like ANT are considered less recalcitrant and easier to degrade than high molecular weight PAHs (4–6 rings) like BaP [10,60]. This typical pattern contrasts with the results observed in the present study. However, other studies using different technologies, such as activated persulfate, has reported the opposite behavior, a higher degradation rate associated with an increased number of rings [61]. Furthermore, BaP has been reported to have a higher affinity for hydroxyl radical oxidation than other PAHs with a similar or even lower number of rings, possibly due to BaP's higher ionization potential [62–64]. In this context, the degradation kinetics of PAHs seem to be primarily influenced by both the molecular structure and the technology employed for their degradation.

Although no statistical tests were applied to compare degradation efficiencies between PAHs or between oxidation processes, future studies involving real samples will address this through formal statistical analysis.

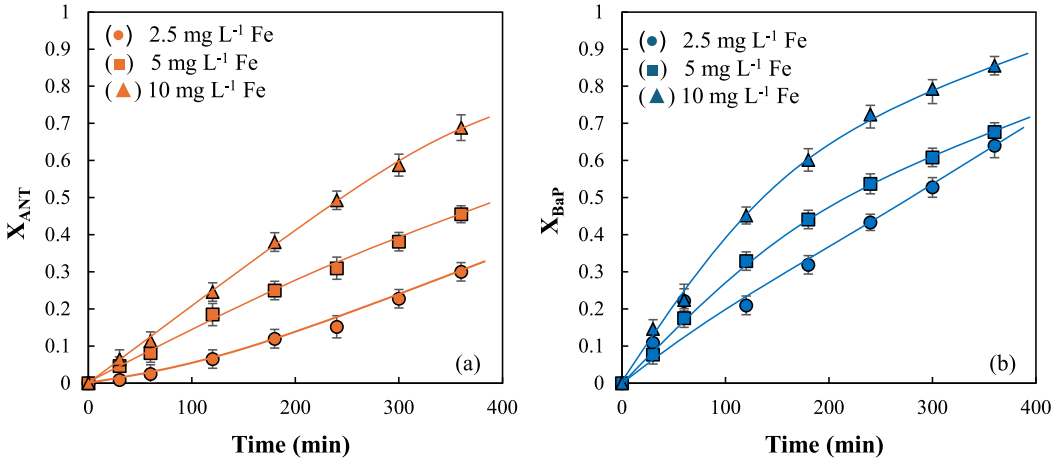

Fig. 6. Influence of iron concentration on the degradation of PAHs in the solar photo-Fenton process (E16, E14, E17) (4500 mg L^{-1} of SDS, 5 mg L^{-1} of ANT, 5 mg L^{-1} of BaP and 120 mg L^{-1} of H_2O_2, pH = 7, mean values ± standard deviations).

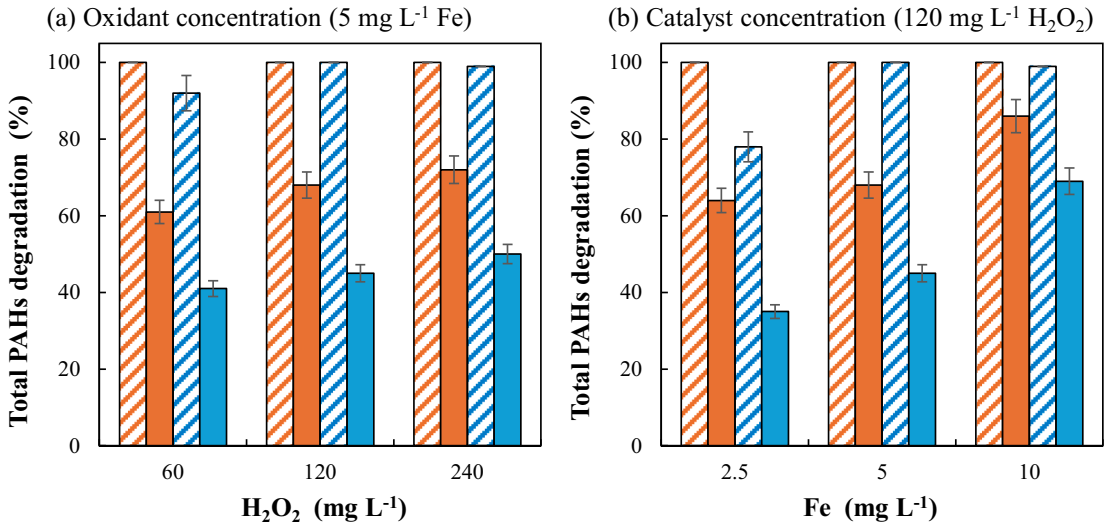

Fig. 7. PAHs degradation at 6 h by Fenton and solar photo-Fenton at different oxidant (a) and catalyst (b) doses. ANT: orange bars; BaP: blue bars. Fenton: stripped bars; solar photo-Fenton: full bars. (For interpretation of the references to color in this figure legend, the reader is referred to the web version of this article.)

3.3.4. *Surfactant stability and reuse of treated emulsions*

The hydroxyl radicals generated during Fenton and simulated solar photo-Fenton processes are not selective and they can lead to the degradation of both the target contaminants and the surfactants present in the emulsion [26,65]. Recovering surfactants from emulsions treated with oxidation processes is crucial both economically and environmentally. Surfactants are used in large concentrations to enhance the solubility of hydrophobic contaminants, and their recovery can significantly reduce operational costs by enabling their reuse in subsequent treatment cycles.

As stated, the concentration of SDS in the emulsion was indirectly measured by quantifying sulfate and sulfonate groups (the anionic part of SDS), while the integrity of the alkyl chain was assessed through total organic carbon (TOC) analysis. The results obtained at the end of the reaction time for the sulfonate groups (SDS) and TOC under different conditions for the Fenton and solar photo-Fenton processes are shown in Fig. 8.

The sulfonate groups of SDS remained almost intact after the oxidation processes under all conditions tested, indicating that the anionic part, essential for its surfactant function, is resistant to the oxidative environment. In the same line, TOC depletion was minimal. Only at the highest concentration of hydrogen peroxide (240 mg L^{-1} of H_2O_2) a slight decrease was observed in SDS concentration (4 % for both processes) and TOC (11 % for Fenton and 9 % for solar photo-Fenton). This slight decrease can be attributed to the higher concentration of hydroxyl radicals generated with increased oxidant dosage. Despite this, the mineralization of the SDS emulsion was negligible, suggesting that the alkyl chain remained largely intact, and the surfactant's overall integrity was preserved after both Fenton and photo-Fenton treatments. Although some oxidation of the alkyl chain might have occurred, low levels of surfactant mineralization are achieved.

The surface tension and critical micelle concentration of the treated emulsions under medium conditions (120 mg L^{-1} of H_2O_2 and 5 mg L^{-1} of Fe) were compared to those of the initial emulsion (prior to the oxidation treatments). This comparison aimed to evaluate whether the surfactant's ability to form micelles remained unchanged, indicating the preservation of its functional integrity after treatments. The surface tension of the treated emulsions remained like that of the initial solution (≈31.8 ± 2.1 mN m^{-1}), and the CMC values obtained after the Fenton and photo-Fenton processes showed <10 % variation compared to the initial emulsion (1925 ± 126 mg L^{-1}). These results confirm the high stability of SDS's surfactant properties following the oxidation

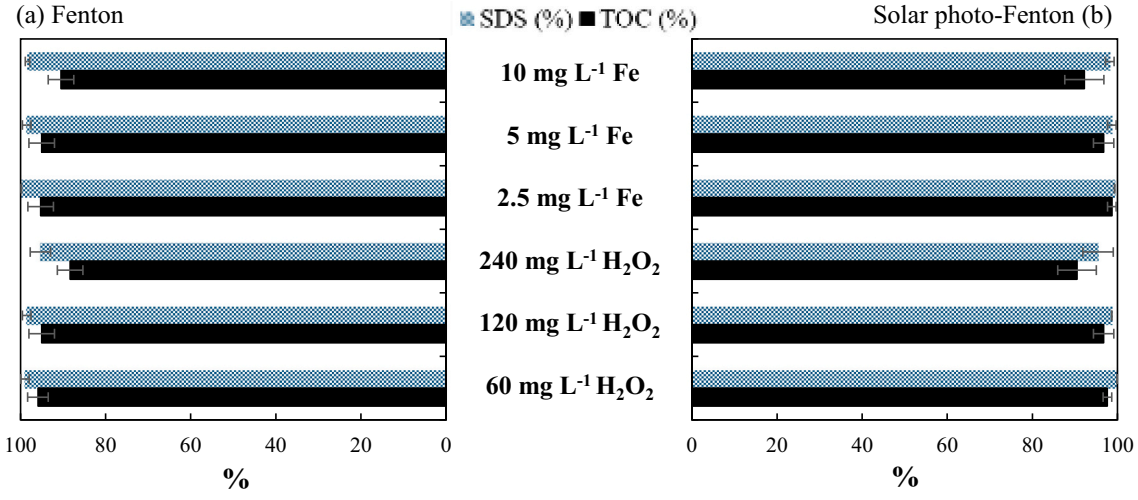

Fig. 8. Surfactant capacity of the emulsion (SDS and TOC) after the (a) Fenton and (b) solar-Fenton processes at different oxidant and catalyst doses. Surface tension and CMC values remain unchanged after oxidation treatments.

treatments. Therefore, the treated emulsions could be reused in subsequent soil washing cycles. In this regard, the presence of H_2O_2 in the emulsions would not pose a problem due to the low content and quick decomposition upon contact with soil. For Fenton treatment, acidifying the emulsion after the soil washing step may be necessary due to the high carbonate content of the soil. Summarizing, both technologies showed promising results in terms of sustainability, allowing the treated emulsion to be reused for solubilizing PAHs in successive processes.

4. Conclusions

This study demonstrates that Fenton and simulated solar photo-Fenton processes effective removes PAHs from aqueous emulsions generated in soil-washing processes, achieving up to 100 and 70 % degradation of BaP and ANT, respectively, in optimized conditions. The Fenton process, operating at pH 3, ensured complete removal of PAHs at H_2O_2 concentrations of 120–240 mg L^{-1} and Fe dosages of 5–10 mg L^{-1}, whereas the solar photo-Fenton process, operating at circumneutral pH and using a ferrioxalate complex to maintain iron in solution, achieved BaP and ANT removal efficiencies of 60–85 % and 35–70 %, respectively, depending on the catalyst dosage.

A key finding is the selective oxidation of PAHs while preserving the integrity of SDS, enabling its potential recovery and reuse. The CMC of the treated emulsions remained at values like the untreated emulsion, confirming that surfactant properties were largely retained. These findings demonstrated that photo-assisted AOPs can be applied for the remediation of PAHs aqueous emulsions, offering a sustainable alternative for treating industrial wastewater and soil-washing effluents. Further optimization, particularly in solar-driven applications, could enhance degradation efficiencies and improve scalability for real-world water treatment scenarios.

CRediT authorship contribution statement

Karima Ayedi: Methodology, Investigation, Data curation. **Yaiza Moreno-De La Fuente:** Methodology, Investigation, Formal analysis, Data curation. **Miguel Herraiz-Carboné:** Writing – original draft, Methodology, Investigation, Formal analysis, Data curation. **Salvador Cotillas:** Validation, Supervision, Funding acquisition, Data curation, Conceptualization. **Marina Prisciandaro:** Writing – review & editing, Supervision, Resources, Funding acquisition, Conceptualization. **Aurora Santos:** Writing – review & editing, Supervision, Resources, Funding acquisition, Conceptualization. **Carmen M. Domínguez:** Writing – review & editing, Supervision, Resources, Funding acquisition, Conceptualization.

Declaration of competing interest

The authors declare that they have no known competing financial interests or personal relationships that could have appeared to influence the work reported in this paper.

Acknowledgments

This research is part of the projects PID2022-137828OB-I00 (EMULREM) and PDC2022-133095-I00 (VAL-REMSURFOX) funded by MCIN/AEI/10.13039/501100011033. Project TEC-2024/ECO-69 (CARESOIL-CM) funded by the Community of Madrid is also acknowledged. Y. Moreno-De la Fuente acknowledges the Spanish State Investigation Agency for the grant PREP2022-000074 funded by MICIU/AEI/10.13039/501100011033 and FSE+.

Appendix A. Supplementary data

Supplementary data to this article can be found online at https://doi.org/10.1016/j.jwpe.2025.107959.

Data availability

Data will be made available on request.

References

[1] M. Vijayanand, et al., Polyaromatic hydrocarbons (PAHs) in the water environment: a review on toxicity, microbial biodegradation, systematic biological advancements, and environmental fate, Environ. Res. 227 (2023).
[2] M.A. Mallah, et al., Polycyclic aromatic hydrocarbon and its effects on human health: an overeview, Chemosphere 296 (2022).
[3] C. Dai, et al., Review on the contamination and remediation of polycyclic aromatic hydrocarbons (PAHs) in coastal soil and sediments, Environ. Res. 205 (2022).
[4] S. Kuppusamy, et al., Remediation approaches for polycyclic aromatic hydrocarbons (PAHs) contaminated soils: technological constraints, emerging trends and future directions, Chemosphere 168 (2017) 944–968.
[5] F. Pardo, et al., Optimization of the application of the Fenton chemistry for the remediation of a contaminated soil with polycyclic aromatic hydrocarbons, J. Chem. Technol. Biotechnol. 91 (6) (2016) 1763–1772.
[6] S.A. Wise, L.C. Sander, M.M. Schantz, Analytical methods for determination of polycyclic aromatic hydrocarbons (PAHs) — a historical perspective on the 16 U.S. EPA priority pollutant PAHs, Polycycl. Aromat. Compd. 35 (2–4) (2015) 187–247.
[7] J. Yan, et al., Photomutagenicity of 16 polycyclic aromatic hydrocarbons from the US EPA priority pollutant list, Mutation Research/Genetic Toxicology and Environmental Mutagenesis 557 (1) (2004) 99–108.
[8] A.T. Lawal, Polycyclic aromatic hydrocarbons. A review, Cogent environmental Science 3 (1) (2017) 1339841, https://doi.org/10.1080/23311843.2017.1339841.
[9] A.B. Patel, et al., Polycyclic aromatic hydrocarbons: sources, toxicity, and remediation approaches, Front. Microbiol. 11 (2020).
[10] M. Cheng, et al., Hydroxyl radicals based advanced oxidation processes (AOPs) for remediation of soils contaminated with organic compounds: a review, Chem. Eng. J. 284 (2016) 582–598.
[11] Z. Zhou, et al., Persulfate-based advanced oxidation processes (AOPs) for organic-contaminated soil remediation: a review, Chem. Eng. J. 372 (2019) 836–851.
[12] R. Yang, et al., Comparison of naphthalene removal performance using H2O2, sodium percarbonate and calcium peroxide oxidants activated by ferrous ions and degradation mechanism, Chemosphere 283 (2021) 131209.
[13] C. Walling, Fenton's reagent revisited, Acc. Chem. Res. 8 (4) (1975) 125–131.
[14] A. Sychiov, V. Isac, Iron compounds and mechanisms of homogeneous catalysis of O-2 and H2O2 activation, as well as oxidation of organic substrates, Usp. Khim. 64 (12) (1995) 1183–1209.
[15] M. Smara, et al., Efficiency of hydrogen peroxide and Fenton reagent for polycyclic aromatic hydrocarbon degradation in contaminated soil: insights from experimental and predictive modeling, Processes 12 (3) (2024).
[16] Y. Gao, et al., Remediation of soil contaminated with PAHs and γ-HCH using Fenton oxidation activated by carboxymethyl cellulose-modified iron oxide-biochar, J. Hazard. Mater. 453 (2023).
[17] M. Mazarji, et al., Decrypting the synergistic action of the Fenton process and biochar addition for sustainable remediation of real technogenic soil from PAHs and heavy metals, Environ. Pollut. 303 (2022).
[18] Y. Gou, et al., Insights into the effects of Fenton oxidation on PAH removal and indigenous bacteria in aged subsurface soil, Environ. Pollut. 298 (2022).
[19] F. Vicente, et al., Improvement soil remediation by using stabilizers and chelating agents in a Fenton-like process, Chem. Eng. J. 172 (2–3) (2011) 689–697.
[20] A. Mojiri, et al., Comprehensive review of polycyclic aromatic hydrocarbons in water sources, their effects and treatments, Sci. Total Environ. 696 (2019).
[21] X. Mao, et al., Use of surfactants for the remediation of contaminated soils: a review, J. Hazard. Mater. 285 (2015) 419–435.
[22] L. Huo, et al., Surfactant-enhanced aquifer remediation: mechanisms, influences, limitations and the countermeasures, Chemosphere 252 (2020) 126620.
[23] C.M. Dominguez, A. Romero, A. Santos, Selective removal of chlorinated organic compounds from lindane wastes by combination of nonionic surfactant soil flushing and Fenton oxidation, Chem. Eng. J. 376 (2019) 120009.
[24] C. Trellu, et al., Remediation of soils contaminated by hydrophobic organic compounds: how to recover extracting agents from soil washing solutions? J. Hazard. Mater. 404 (2021) 124137.
[25] J. Rosas, et al., Soil remediation using soil washing followed by fenton oxidation, Chem. Eng. J. 220 (2013) 125–132.
[26] J.K. Saxe, H.E. Allen, G.R. Nicol, Fenton oxidation of polycyclic aromatic hydrocarbons after surfactant-enhanced soil washing, Environ. Eng. Sci. 17 (4) (2000) 233–244.
[27] S. Safa, M.R. Mehrasbi, Investigating the photo-Fenton process for treating soil washing wastewater, J. Environ. Health Sci. Eng. 17 (2019) 779–787.
[28] R.D. Villa, A.G. Trovó, R.F.P. Nogueira, Soil remediation using a coupled process: soil washing with surfactant followed by photo-Fenton oxidation, J. Hazard. Mater. 174 (1–3) (2010) 770–775.
[29] L.O. Conte, A.V. Schenone, O.M. Alfano, Photo-Fenton degradation of the herbicide 2,4-D in aqueous medium at pH conditions close to neutrality, J. Environ. Manag. 170 (2016) 60–69.
[30] L.O. Conte, et al., Solar-assisted oxidation of organochlorine pesticides in groundwater using persulfate and ferrioxalate, Environ. Pollut. 343 (2024).
[31] L.O. Conte, et al., Vis LED photo-Fenton degradation of 124-trichlorobenzene at a neutral pH using ferrioxalate as catalyst, Int. J. Environ. Res. Public Health 19 (15) (2022) 9733.

[32] I.N. Dias, et al., Fluorene oxidation by solar-driven photo-Fenton process: toward mild pH conditions, Environ. Sci. Pollut. Res. 25 (28) (2018) 27808–27818.
[33] P.K. Singa, et al., Photo-Fenton process for removal of polycyclic aromatic hydrocarbons from hazardous waste landfill leachate, Int. J. Environ. Sci. Technol. 18 (11) (2021) 3515–3526.
[34] U.J. Ahile, et al., A review on the use of chelating agents as an alternative to promote photo-Fenton at neutral pH: current trends, knowledge gap and future studies, Sci. Total Environ. 710 (2020) 134872.
[35] L. Clarizia, et al., Homogeneous photo-Fenton processes at near neutral pH: a review, Appl. Catal. B Environ. 209 (2017) 358–371, https://doi.org/10.1016/j.apcatb.2017.03.011.
[36] A. Checa-Fernández, et al., Remediation of real soils polluted with pesticides by activated persulfate and surfactant addition, J. Water Process. Eng. 53 (2023) 103829, https://doi.org/10.1016/j.jwpe.2023.103829.
[37] L. Wang, H. Wu, D. Deng, Role of surfactants in accelerating or retarding persulfate decomposition, Chem. Eng. J. 384 (2020) 123303.R.
[38] R. Khalladi, et al., Surfactant remediation of diesel fuel polluted soil, J. Hazard. Mater. 164 (2–3) (2009) 1179–1184.
[39] S. Dini, et al., The physicochemical and functional properties of biosurfactants: a review, Molecules 29 (11) (2024) 2544.
[40] M. Tiwari, D.B. Tripathy, Soil contaminants and their removal through surfactant-enhanced soil remediation: a comprehensive review, Sustainability 15 (17) (2023) 13161.
[41] C.M. Dominguez, et al., Remediation of HCHs-contaminated sediments by chemical oxidation treatments, Sci. Total Environ. 751 (2021) 141754.
[42] R. García-Cervilla, et al., Compatibility of nonionic and anionic surfactants with persulfate activated by alkali in the abatement of chlorinated organic compounds in aqueous phase, Sci. Total Environ. 751 (2021) 141782.
[43] L.O. Conte, G. Legnettino, D. Lorenzo, S. Cotillas, M. Prisciandaro, A. Santos, Degradation of Lindane by persulfate/ferrioxalate/solar light process: influential operating parameters, kinetic model and by-products, Appl. Catal. B Environ. 324 (2023) 122288.
[44] BOE, Ley 5/2002, de 3 de junio, sobre vertidos de aguas residuales industriales a los sistemas públicos de saneamiento, 2002.
[45] B.N. Giménez, et al., Reaction kinetics formulation with explicit radiation absorption effects of the photo-Fenton degradation of paracetamol under natural pH conditions, Environ. Sci. Pollut. Res. 28 (19) (2021) 23946–23957.
[46] G. Eisenberg, Colorimetric determination of hydrogen peroxide, Ind. Eng. Chem. Anal. Ed. 15 (5) (1943) 327–328.
[47] ISO, I.O.f.S, ISO6332: Water Quality — Determination of Iron — Spectrometric Method Using 1,10-Phenanthroline, 1988.
[48] E. Jurado, et al., Simplified spectrophotometric method using methylene blue for determining anionic surfactants: applications to the study of primary biodegradation in aerobic screening tests, Chemosphere 65 (2) (2006) 278–285.
[49] S. Paria, K.C. Khilar, A review on experimental studies of surfactant adsorption at the hydrophilic solid–water interface, Adv. Colloid Interf. Sci. 110 (3) (2004) 75–95.
[50] R. Garcia-Cervilla, et al., Partition of a mixture of chlorinated organic compounds in real contaminated soils between soil and aqueous phase using surfactants: influence of pH and surfactant type, J. Environ. Chem. Eng. 9 (5) (2021) 105908.
[51] M.S. Rodríguez-Cruz, M.J. Sanchez-Martin, M. Sanchez-Camazano, A comparative study of adsorption of an anionic and a non-ionic surfactant by soils based on physicochemical and mineralogical properties of soils, Chemosphere 61 (1) (2005) 56–64.
[52] H.L. Silcock, H. Stephen, T. Stephen, Solubilities of Inorganic and Organic Compounds, Pergamon Press, 1963.
[53] C. Laurent, et al., Milk−blood transfer of 14C-tagged polycyclic aromatic hydrocarbons (PAHs) in pigs, J. Agric. Food Chem. 49 (5) (2001) 2493–2496.
[54] R. Venkatadri, R.W. Peters, Chemical oxidation technologies: ultraviolet light/hydrogen peroxide, Fenton's reagent, and titanium dioxide-assisted photocatalysis, Hazard. Waste Hazard. Mater. 10 (2) (1993) 107–149.
[55] P.C. Marinosa, et al., Real soil treatment by chemical oxidation: hydrogen peroxide application, in: Recent Advances in Fluid Mechanics and Heat&Mass Transfer, 2011 (Florence, Italy).
[56] A. Santos, et al., Mineralization lumping kinetic model for abatement of organic pollutants using Fenton's reagent, Catal. Today 151 (1–2) (2010) 89–93.
[57] E. Neyens, J. Baeyens, A review of classic Fenton's peroxidation as an advanced oxidation technique, J. Hazard. Mater. 98 (1) (2003) 33–50.
[58] L. Ge, et al., Aqueous photochemical degradation of hydroxylated PAHs: kinetics, pathways, and multivariate effects of main water constituents, Sci. Total Environ. 547 (2016) 166–172.
[59] L. Ge, et al., Aquatic photochemistry of fluoroquinolone antibiotics: kinetics, pathways, and multivariate effects of main water constituents, Environ. Sci. Technol. 44 (7) (2010) 2400–2405.
[60] S. Jonsson, et al., Degradation of polycyclic aromatic hydrocarbons (PAHs) in contaminated soils by Fenton's reagent: a multivariate evaluation of the importance of soil characteristics and PAH properties, J. Hazard. Mater. 149 (1) (2007) 86–96.
[61] I. Bouzid, et al., Compatibility of surfactants with activated-persulfate for the selective oxidation of PAH in groundwater remediation, J. Environ. Chem. Eng. 5 (6) (2017) 6098–6106.
[62] K. Nam, W. Rodriguez, J.J. Kukor, Enhanced degradation of polycyclic aromatic hydrocarbons by biodegradation combined with a modified Fenton reaction, Chemosphere 45 (1) (2001) 11–20.
[63] V. Flotron, et al., Removal of sorbed polycyclic aromatic hydrocarbons from soil, sludge and sediment samples using the Fenton's reagent process, Chemosphere 59 (10) (2005) 1427–1437.
[64] S. Lundstedt, Y. Persson, L. Öberg, Transformation of PAHs during ethanol-Fenton treatment of an aged gasworks' soil, Chemosphere 65 (8) (2006) 1288–1294.
[65] K. Choi, S. Bae, W. Lee, Degradation of pyrene in cetylpyridinium chloride-aided soil washing wastewater by pyrite Fenton reaction, Chem. Eng. J. 249 (2014) 34–41.